LDA Characterization of the Velocity Field around a Growing and Rising Bubble in Shear-thinning Fluid

doi: 10.15255/CABEQ.2013.1891

W. Fan* **and X. Yin**
School of Chemistry and Chemical Engineering,
Tianjin University of Technology, Tianjin 300384, P. R. China

Original scientific paper
Received: November 18, 2013
Accepted: July 23, 2014

Laser Doppler anemometry (LDA) has been employed to quantify the liquid velocity field around a single bubble in its generating and accelerating stage in carboxymethylcellulose (CMC) aqueous solution. The instantanoues velocities were treated by Reynolds time-averaged method, and mean velocities and its contours in both axial and radial directions were investigated. The results show that in vertical direction, the flow field characteristics of the liquids around the bubble are determined by bubble formation-rise mechanism, whereas in horizontal direction they are governed by the relative position with the bubble shear radius. The contours of axial and radial mean velocity in the test section take on the shapes of inverted trapezoid and butterfly forewing, respectively.

Key words:
bubble formation, velocity field, shear-thinning, laser Doppler anemometry

Introduction

Multiphase flow in non-Newtonian fluids have received considerable attention because of their inherent scientific appeal and importance in industrial application, such as chemical, biochemical, environmental and petrochemical processes.[1,2] In typical equipment employing bubbly flow, such as bubble columns and bioreactors, the bubble formation process is frequently encountered and will cause marked variations in the flow fields as well as the bubble dynamics in non-Newtonian fluids. Not only the shape, velocity, and track of the bubble are affected by the flow fields around a growing bubble, but also coalescence can take place via the interaction between bubbles under formation, consequently leading to a significant impact on the hydrodynamics as well as the mass and heat transfer between gas-liquid phases. Adequate understanding of the flow structure surrounding single bubble rising in non-Newtonian fluid is therefore essential to optimize gas-liquid equipment design, as well as to access an overall insight into the bubble coalescence mechanism.

Compared to the extensive research on bubble formation in Newtonian fluids,[3] much less is known about the topic in non-Newtonian fluids. The earlier investigations were mainly in experimental visualization of the volume of bubble.[4] Further, a simplified equation ($V = C(Q^2/g)^{3/5}$) of bubble volume under constant gas flow rate was correlated without considering rheological characteristics of the fluid.[5,6] Based on the difference in various stages of bubble formation, a two-stage spherical model was proposed,[7] but could only be applied to low concentration system owing to the neglect of gas momentum and the assumption of spherical bubble. Terasaka and Tsuge[8–10] investigated experimentally the influence of chamber volume, orifice diameter, gas flowrate and the rheological properties of fluids on bubble volume and bubble shape, and developed an improved non-spherical model for bubble formation. On the basis of the non-spherical model, Li[11] and Li *et al*.[12] advanced a novel model to predict the instantaneous size, shape and frequency during bubble formation process by considering the influence of in-line interactions between two consecutive bubbles due to the fluid memory effects. From the view of control mechanism of bubble formation, Favelukis and Albalak[13] put forward a dynamic-control spherical model for bubble growth on the assumption that bubble was firstly controlled by dynamics and then by mass transfer. According to their results, the bubble radius changed as an exponential function of time for the initial stage, but was proportional to the square root for the late stage. A similar research was reported by emphasizing the effect of gas diffusion in fluid, which indicated that, all else being equal, bubbles in power law liquids grew slower the smaller the characteristic exponent.[14] By introducing state equation of ideal gas, Martín *et al*.[15,16] studied the two stages of growth and rise of bubble formation in both Newtonian and non-Newtonian fluids, and proposed a non-spherical model for the prediction of bubble volume, su-

* Corresponding author: e-mail: wyfan@tjut.edu.cn.

perficial area, and bubble shape, which could well estimate bubble shapes and generation times during the growth stage and during the first step of the rising stage. Fan *et al*.[17] applied laser image technique to reveal the impact of the solution properties, orifice diameter on the bubble detachment volume and revealed that bubble detachment volume increased with solution concentration and orifice diameter. Recently, Vélez-Cordero and Zenit[18] devoted to the bubble cluster formation in power-law shear-thinning fluids found that the mean rise velocity of the bubbles was larger than that of an individual bubble.

Besides, previous experimental research is focused mainly on the bubble wake formed behind the leading bubble and its effect on trailing bubble, as well as its difference from that in Newtonian fluids. Hassager[19] first observed that a negative wake in non-Newtonian fluids pushed the liquid away from the bubble Subsequently, by means of Laser Doppler Anemometry (LDA), Bisgaard and Hassager[20] concluded that a negative wake was induced by elasticity, which usually has the opposite-direction effect to the inertial force. This peculiar phenomenon has also been observed for spheres falling in viscoelastic liquids.[21] Furthermore, Frank and Li[22,23] found the coexistence of three distinct zones around bubbles rising in polyacrylamide (PAM) solutions: A central downward flow behind the bubble (negative wake), a conical upward flow surrounding the negative wake zone, and an upward flow zone in front of the bubble. The three zones were further verified while experimentally measuring the flow fields around a solid sphere settling down in the same fluids.[24] Pillapakkam *et al.*[25] performed direct numerical simulation to investigate the transient and steady motion of the bubbles rising in a viscoelastic fluid, and revealed that the wake structure was closely related to a critical bubble volume. Sousa *et al*.[26] conducted experimentally the interaction between consecutive Taylor bubbles rising in non-Newtonian solutions via sets of laser diodes/photocells and Particle Image Velocimetry (PIV). According to Sousa, for the less concentrated CMC solutions, the interaction between Taylor bubbles was similar to that found in Newtonian fluids, and for the most concentrated CMC solution, a negative wake formed behind the Taylor bubbles. Lin and Lin[27] investigated experimentally the coalescence mechanism of in-line two-unequal bubbles rising in polyacrylamide (PAM) solution using Particle Image Analyzer (PIA), and proposed that the acceleration of the trailing bubble to the leading one is caused respectively by the negative pressure at the leading bubble wake, a reducing viscosity by shear-thinning, and a circulated upward flow by viscoelasticity. Fan *et al*.[28] focused on the interaction between two parallel rising bubbles by analyzing the velocity field around bubbles using PIV. Zhang *et al*.[29] applied an improved level set method to simulate the motion of deformable bubble in shear-thinning fluids, and found that two separated zones in the vortex-shedding regime formed as a region of wake with high viscosity appeared. Li *et al*.[30] explored experimentally a hollow cylindrical low viscosity region around the bubble wake and a high viscosity region in the central bubble wake around a rising bubble in CMC fluids. From turbulent kinetic energy (TKE) point of view, Li *et al*.[31] investigated the flow characteristics of fluid induced by a chain of bubbles rising in non-Newtonian fluids, and discovered that the TKE profiles were almost symmetrical along the column center and showed higher values in the central region of the column. Most recently, Amirnia *et al*.[32] studied the free rise of small bubble in xanthan gum and CMC solutions, and found the distinct differences of bubble shape and its rising path between the smaller bubble and the larger one, but no discontinuity in the rise velocity over the experimental bubble volume range.

Nevertheless, few papers have been devoted to the velocity flow field around an under-formation bubble. To obtain a detailed velocity distribution around a bubble, both in former growing period and in subsequent rising stage, it is critical to confirm the overwhelming mechanism of bubble formation and the theory of bubble-bubble interaction as well as coalescence during bubble generation. On the other hand, despite the disadvantage of time-consuming, Laser Doppler Anemometry (LDA) has such obvious advantages as high resolution, non-interference, quick response, and has become one of the most favored tools for investigating the multiphase flow application compared to the conventional one-point measurement methods, such as Pitot tube, hot wire anemometry, etc. The LDA is more robust for optical disturbances and offers full-field measurements even at higher mixture velocities, compared with PIV technology, which, however, becomes ineffective when close to the interface at higher mixture velocities due to large reflections created by interfacial waves and droplets.[33] In this work, the flow field near the bubble growing in shear-thinning fluid was experimentally investigated by analysis of the mean velocity and its contour in both radial direction and axial direction using LDA.

Experimental

Test section

In present experiments, the single bubble rose straightly upward with no obvious oscillation, and its shape became axisymmetrical with the axis of the

vertical line passing through orifice centre. Thus, only velocities in y direction and z direction need to be considered. Consequently, the test section was selected as a rectangular channel with the following geometric dimensions: width (in y direction) W: 1.60 cm, height (in z direction) H: 7.85 cm, as illustrated in Fig. 1. Particularly, to avoid the influence of refraction of Plexiglas section with orifice on the laser beam, the origin (O) of the co-ordinate system was fixed at the intersection point between the vertical line passing through orifice center and the horizontal line 2 mm above orifice. Note that only two-dimensional velocity components along the $\{y, z\}$ axes, denoted as $\{v, w\}$ were used.

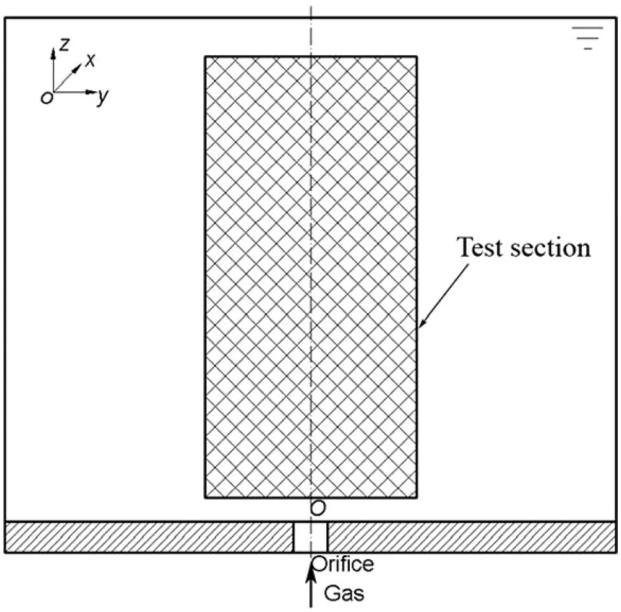

Fig. 1 – *Schematic diagram of test section*

Experimental setup

The experimental facility consisted of two parts: bubble generation system and LDA measurement system, as shown in Fig. 2. Bubble generation system included a Plexiglas square tank with dimensions of 15×15×50 cm, which was considered large enough to neglect the effect of the wall on the shape and size of bubbles. A Plexiglas plate with dimension of 15.0×5.0×1.0 cm, having a polished orifice (inside diameter 2.0 mm) in its centre, was placed inside the tank 10 cm above the bottom for generating bubbles. The stainless tubing with inside diameter of 2.0 mm linked the nitrogen cylinder, rotameter and orifice. Nitrogen pressure was maintained at slightly above 0.1 MPa by adjusting a regulation valve, thus the gas flow rate could be shown accurately by the calibrated rotameter. Nitrogen bubbles are always generated synchronously at stable frequency from the submerged orifice by properly adjusting the gas flow rate.

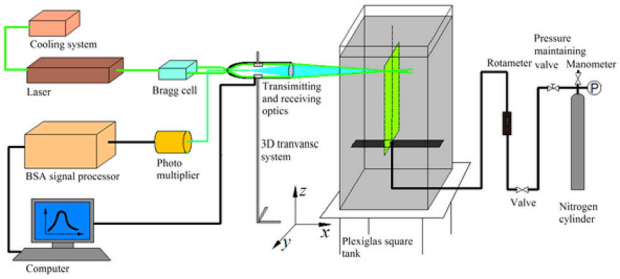

Fig. 2 – *Schematic diagram of experimental system*

The LDA equipment (DANTEC, Fiber flow series 60X, Denmark) involved a 5W water-cooled argon-ion laser source, a multicolor beam separator, a fiber optic probe with a focal length of 310 mm and a multicolor receiver coupled with a traversing coordinate, Dantec 57N21signal processor, and a PC using the Burst Spectrum Analyzer (BSA) Flow Software 2.1 for data acquisition. The back-scattering mode in a cell-free system was employed, the vertical component was determined with green (λ = 514.5 nm) beams and the horizontal one with blue (λ = 488 nm) beams. Distilled water was used as a working solvent to avoid disturbance of LDA system, and spherical glass particles of 10 μm in diameter (density: $1.5 \cdot 10^3$ kg m^{-3}) were seeded and homogeneously distributed throughout the solution. These seeding particles carried by the liquid reflected the laser light toward the photo-detector probe. Hence, the liquid velocity was measured with the LDA equipment. Moreover, a pre-shift frequency of 40 kHz was used, and the time series obtained were 3 minutes long.

Experimental condition

The experiments were performed at 293.15 ± 0.1 K under the following conditions: orifice internal diameter of 2.0 mm; gas flow rate (at 0.1 MPa pressure) of 0.5 mL s^{-1}. Two shear-thinning fluids were applied in this work: 0.15 wt% of CMC in pure water, marked with 0.15 % CMC (1); and 0.15 wt% of CMC in a mixture of 76.9–23.1 % water-glycerol, marked with 0.15 % CMC (2). The rheological characteristics of CMC aqueous solutions were measured by Rheometer of StressTech (REOLOGICA Instruments AB, Sweden), and the results suggested that the behavior of shear-thinning of the fluid can be described very well by Carreau model (Eq. (1)) within experimental shear range from 2.0 to 60. The result is shown in Fig. 3 and Table 1.

$$\frac{\eta - \eta_\infty}{\eta_0 - \eta_\infty} = \left[1 + (\lambda\dot{\gamma})^2\right]^{(n-1)/2} \qquad (1)$$

where η_0, η_∞, λ and n are zero-shear viscosity, infinite shear viscosity, time constant and flow index, respectively.

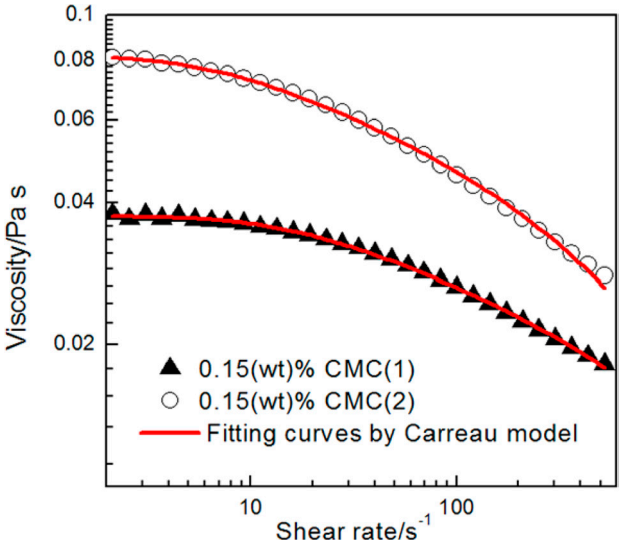

Fig. 3 – *Rheological properties of CMC solutions*

Table 1 – *Rheological parameters of non-Newtonian CMC solutions*

Fluid	η_0 /Pa s	η_∞ /Pa s	λ /s	n
0.15 % CMC (1)	0.03762	0.001	0.068962	0.80767
0.15 % CMC (2)	0.08282	0.001	0.101070	0.73567

Note that in the present conditions, the ellipsoid bubble with volume from 0.249 to 0.286 cm^3 always generates at a very small frequency from 1.75 to 2.01, which could be calculated by gas flow rate and bubble volume. Thus, the interaction between two successive bubbles becomes negligible and the characteristics of the velocity fields surrounding a growing and rising bubble could be specified. Consequently, Reynolds number ranging from 4.9 to 38.2 could be calculated by Eq. (2).

$$Re = \frac{\rho u_b d_e}{\eta} \tag{2}$$

where ρ, u_b and d_e are fluid density, bubble rising velocity, and bubble equivalent diameter, respectively.

Results and discussion

The instantaneous velocity time series of liquids obtained from LDA, with their strong pulsation as shown in Fig. 4, were calculated by Reynolds time-averaged method through MatLab software to acquire the mean velocity in axial and radial direction in the test section. The axial and radial mean velocity (denoted as w and v in Fig. 5 and Fig. 7) distributions and their corresponding contours were then discussed to discover the interaction mechanism between bubble formation and fluid flow.

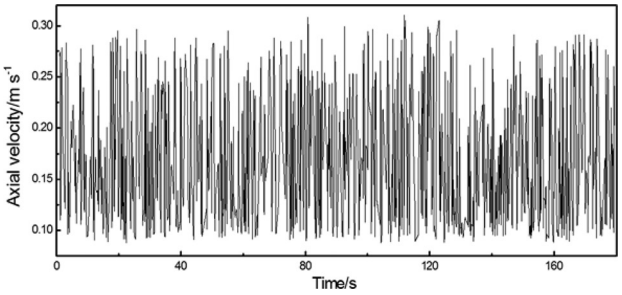

Fig. 4 – *Part of time series of axial velocity*

Axial mean velocity distribution

Plots of the time-averaged axial component of velocity in 0.15 % CMC (1) and 0.15 % CMC (2) solutions are shown in Fig. 5(A) and 5(B), respectively. Note that only the right lateral section from the origin of coordinates ($y > 0$) was plotted instead of a full section due to the axisymmetrical characteristic of flow field, which caused the bubble rising in a vertical path without oscillation or deflection. As a main contributor to the total velocity magnitude, the axial mean velocity performs differently according to the height ranging from bubble formation to its rising. In case of low height (e.g. z = 0~1.3 cm), as bubble shape evolution during its generation process presented in Fig. 6, bubble formation undergoes two stages: expansion and elongation, which are mainly governed by surface tension and buoyancy, respectively.[17] In this case, bubble firstly expands spherically (0 ms ~ 40 ms) and then stretches vertically (40 ~ 160 ms), as shown in Fig. 6. However, the radial expansion rate of bubble surface reduces with the increase in bubble volume for constant flow rate condition, and meanwhile the elongation rate of bubble increases quickly due to the continuously increasing buoyancy, as shown in Fig. 6. Therefore, in the zone near the central axis (e.g. y = 0, 1.0 mm), the axial mean velocity of the liquid is declining followed by rising with the increase in the height, since the liquid always flows upward, as shown in Fig. 5 (*left*). However, in case of middle distance (e.g. y = 2.0, 3.0, 4.0, 5.0 mm), the angle between total velocity and its axial component becomes obvious and reduces gradually with the height along bubble surface boundary, consequently, the axial velocity always keeps rising with the height. However, in case of large distance (e.g. y = 6.0, 7.0, 8.0 mm), the liquid motion is slightly influenced by bubble formation since the distance is larger than bubble shear radius (about 5.0 mm), as shown in Fig. 6, so the axial component tends to almost maintain stable. On the other hand, axial component appears to have Gaussian distribution along the central axis in horizontal direction, although a jump occurs in velocity at the lower position (z = 8.0 mm),

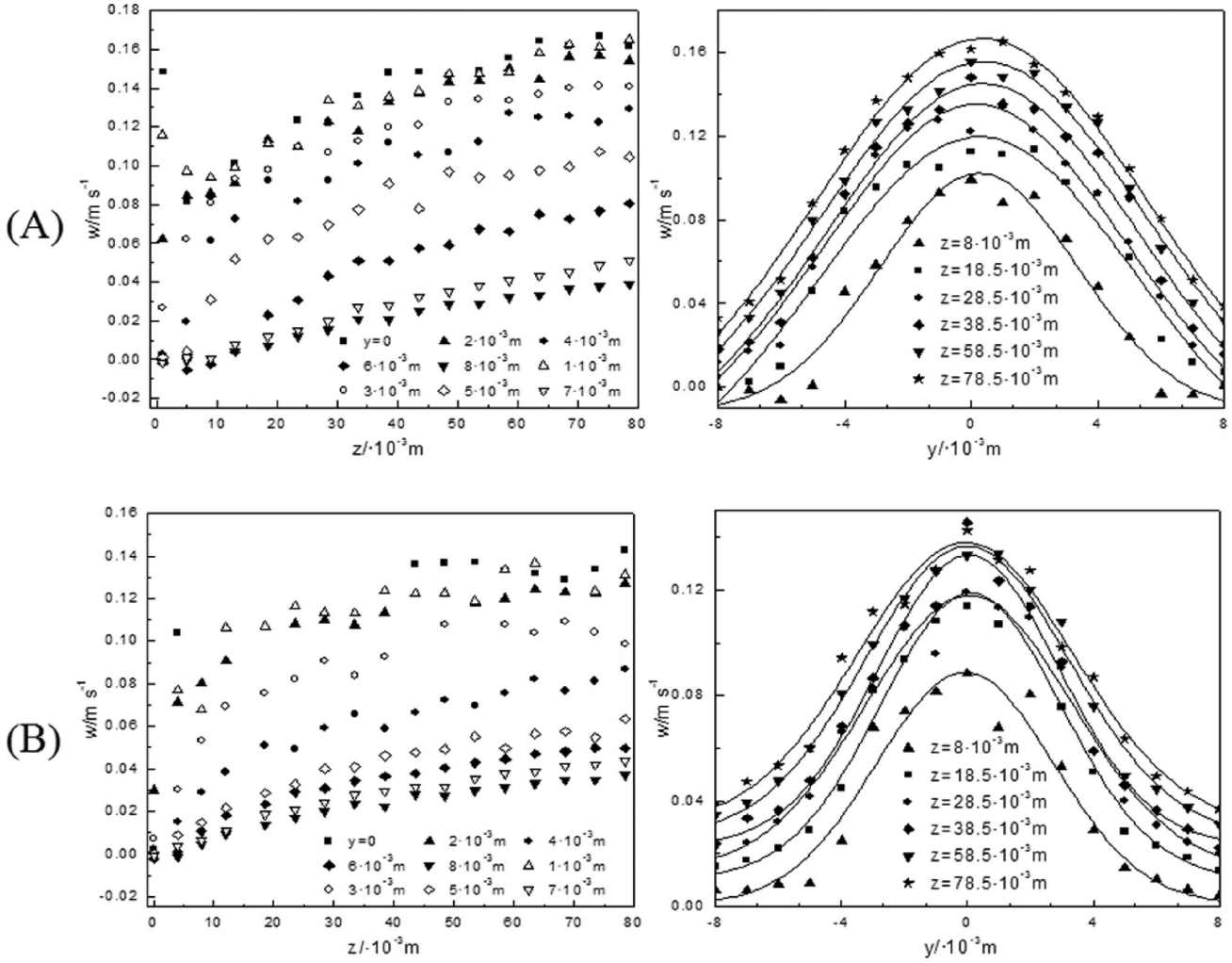

Fig. 5 – *Variation of axial mean velocities in 0.15 % CMC (1) (A) and 0.15 % CMC (2) (B) with height (left) and horizontal position (right)*

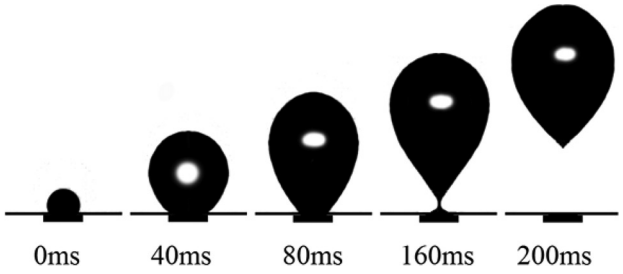

Fig. 6 – *Bubble shape evolutions at different times*

caused by bubble deformation during its growth process, as presented in Fig. 5 (*right*). However, in Newtonian fluids,[34] a one-dimensional model rather than Gaussian distribution was applied to present the radial profile of average liquid velocity with the assumption that liquid velocity presents only in axial direction. Further, the Gaussian curve for higher position is located above that for the lower one, and the reasons can be attributed to the results of bubble acceleration after departing from orifice.

Radial mean velocity distribution

Fig. 7 illustrates that radial mean velocity of liquid varies with height and horizontal position. As one of the components of velocity, the radial velocity of liquid around bubble is closely related to the dynamics behavior of bubble. Hence, within the range of bubble formation (e.g. z = 0~1.3 cm), radial velocity of liquid varies depending on different horizontal distance from the central axis: firstly, in case of small distance (e.g. y = 0, 1.0 mm), the liquid in front of bubble always flows upward, so its radial velocity approaches zero. Secondly, in case of middle distance (e.g. y = 2.0, 3.0, 4.0, 5.0 mm), bubble surface growth rate and the angle between total velocity and axial component, decreases with vertical height in the expansion stage, whereas bubble's deformation takes place mainly in axial direction during the elongation stage. Consequently, radial velocity of liquid decreases with the height involved. Finally, in case of large distance (e.g. y = 6.0, 7.0, 8.0 mm), radial velocity of liquid be-

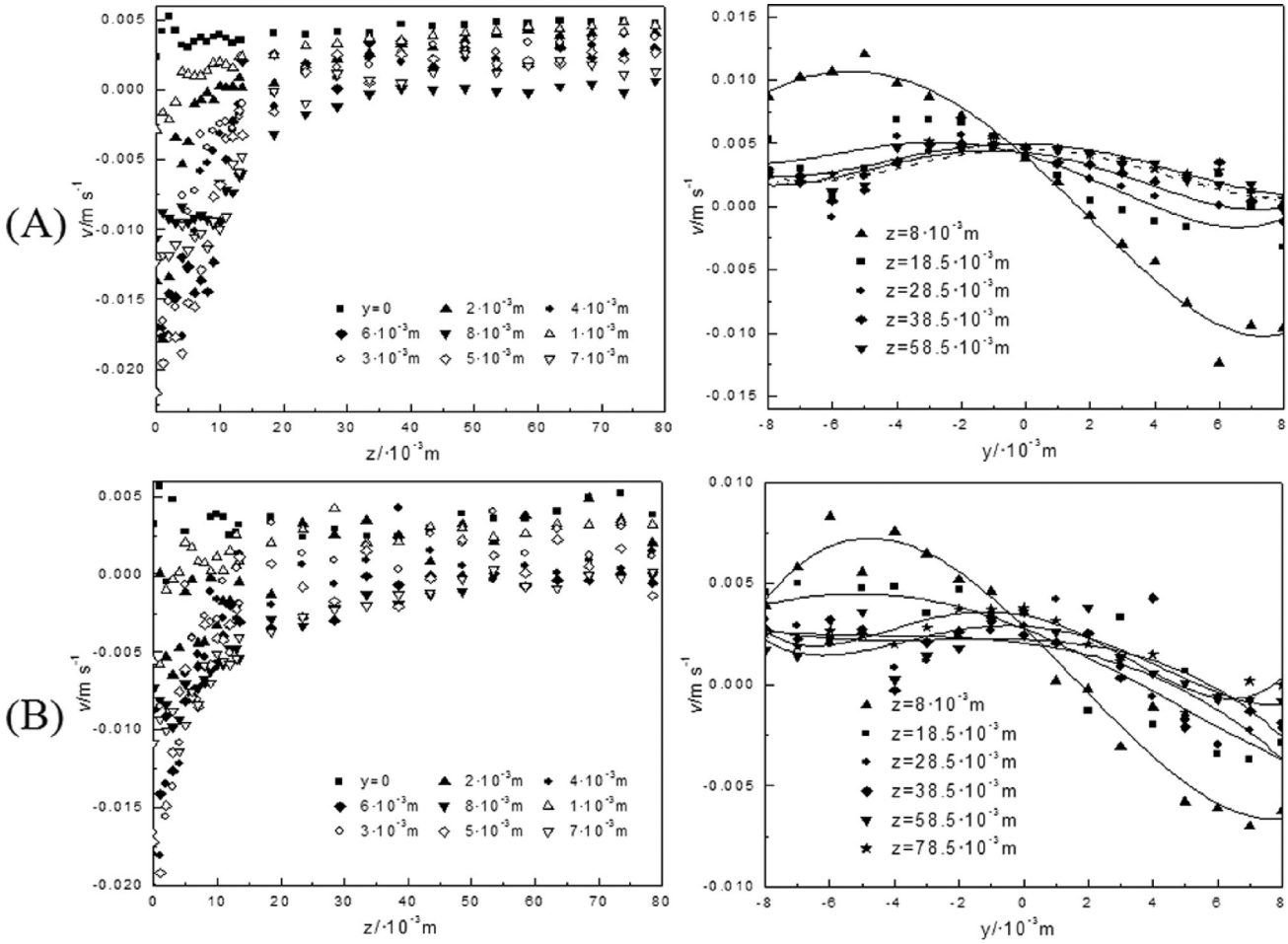

Fig. 7 – *Variation of radial mean velocities in 0.15 % CMC (1) (A) and 0.15 % CMC (2) (B) with height (left) and horizontal position (right)*

comes close to zero again, for the liquid is hardly induced by bubble formation or rise under experimental bubble radius condition, as shown in Fig. 7 (*left*). However, within the range of bubble rise (e.g. z = 1.3 cm ~ 7.85 cm), bubble starts to rise and gradually obtains its terminal shape and rise velocity, and the liquid moves straightly upward due to the periodic shear of the rising bubble. Thus, the radial velocity of the surrounding liquid approaches zero with increase in the height. However, in horizontal direction, the radial velocity firstly increases and then declines with the horizontal distance, which variation extent is decreasing with the rise in height, as shown in Fig. 7 (*right*). It is worth noting that the measured points of radial velocities, especially in low positions, become more scattered due to the fluid's complex characteristics compared with that in Newtonian fluids.[34]

Mean velocity contours

The mean velocity contour of both axial and radial components on test section is plotted and shown in Fig. 8. It is clearly shown that the influence domain of liquid caused by bubble motion becomes wider with the increase in height, owing to the fact that bubble volume continuously increases with height in that stage. Consequently, the overall profile of axial velocity contours emerges as an inverted trapezoidal shape, with top and bottom width of about 12.0 mm and 6.0 mm, respectively. However, this particular shape becomes a regular zone with the same width at top and bottom in Newtonian fluids[34] because of the larger frequency and higher measuring points. Further, the axial velocity component reaches maximum value near the center axis and then declines symmetrically with both left and right direction. But this descending gradient of axial velocity drops with the height due to the rise in the domain width influenced, as shown in Fig. 8 (*left*). Moreover, the maximum radial velocity appears near both sides of orifice (y = ±3.0 mm) due to the strong radial compression and later axial pushing of bubble during its generating process. It is noteworthy that the radial component begins to drop with the increase in both vertical height and horizontal distance until its contour dies away at the height (z = 11.0 mm), consequently, the overall pro-

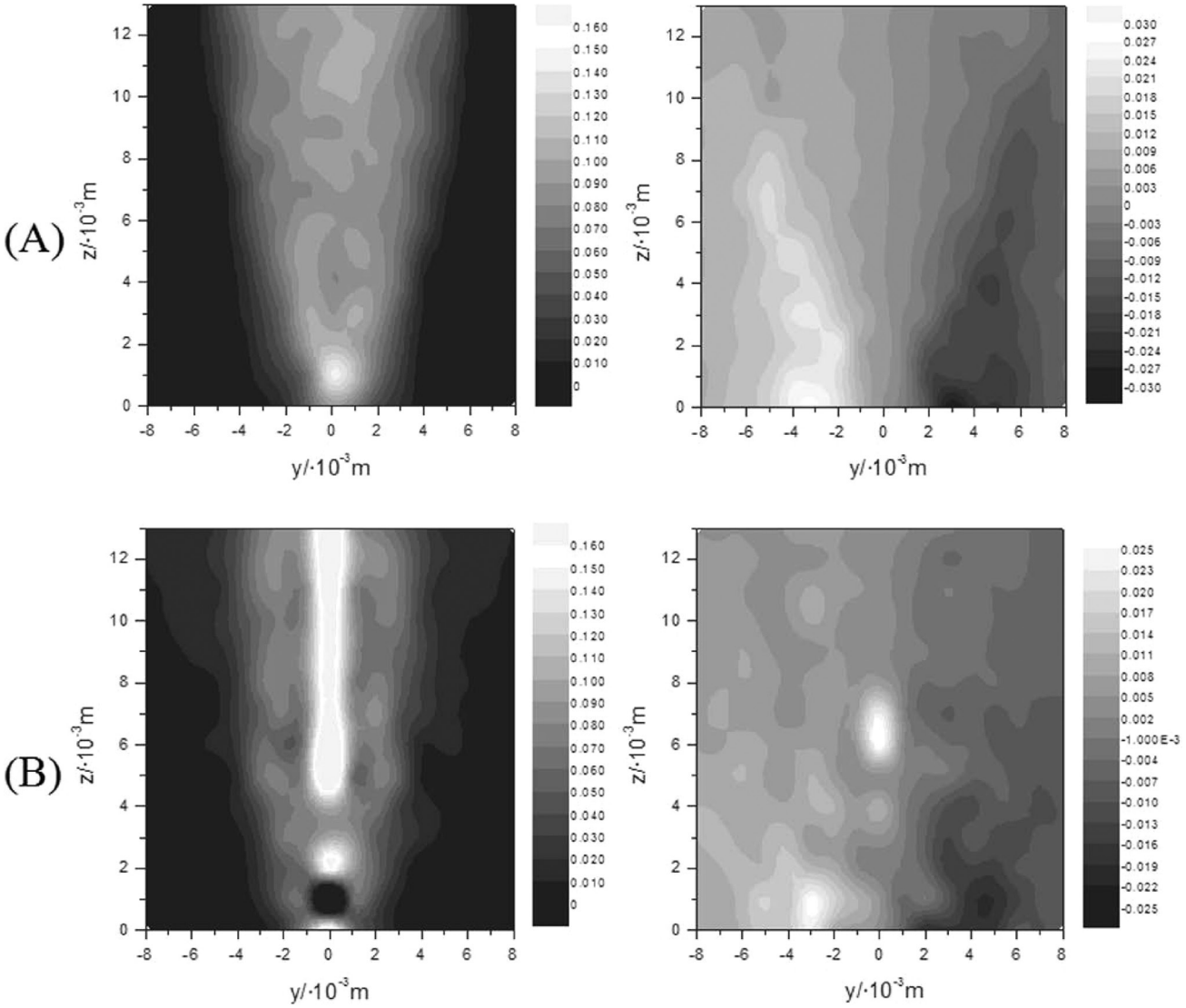

Fig. 8 – *Contours of axial (left) and radial (right) mean velocities on the tested section in 0.15 % CMC (1) (A) and 0.15 % CMC (2) (B)*

file of radial velocity contour takes on the shape of a butterfly forewing, as shown in Fig. 8 (*right*).

Conclusions

Both liquid instantaneous velocity and mean velocity near single bubble forming and rising in non-Newtonian CMC aqueous solutions under low gas flow rate conditions have been measured experimentally by Laser Doppler Anemometry. The disturbance of fluid surrounding the bubble was investigated by means of statistical method, and the conclusions are as follows:

Throughout the rising process, there might exist a cylindrical channel, vertical to the test section and axisymmetrical with the central axis line passing through orifice center, since bubble in the CMC aqueous solution rises steadily along a straight path with no swinging motions. Within the lower region of bubble formation, axial mean velocity increases with height above the origin of coordinate, and shows Gauss distribution in horizontal direction. Further, radial mean velocity reduces to a constant value with the rise in height, whereas in horizontal direction, exhibits an oscillation to a certain degree with the distance from the central axis. The contours of axial and radial mean velocity, respectively, take on the shape of inverted trapezoid and butterfly forewing.

ACKNOWLEDGMENTS

Authors wish to express their appreciation for the financial support of the National Natural Science Foundation of China (21076139, 21106106), Tianjin Natural Science Foundation (12JCQNJC03700), and Foundation of Tianjin Educational Committee of China (20100508).

References

1. *Shah, Y. T., Kelkar, B. G., Godbole, S. P., Deckwer, W. D.,* AIChE J. **28** (1982) 353. http://dx.doi.org/10.1002/aic.690280302
2. *Kilonzo, P. M., Margaritis, A.,* Biochem. Eng. J. **17** (2004) 27. http://dx.doi.org/10.1016/S1369–703X(03)00121–9
3. *Kulkarni, A. A., Joshi, J. B.,* Ind. Eng. Chem. Res. **44** (2005) 5873. http://dx.doi.org/10.1021/ie049131p
4. *Räbiger, N., Vogelpohl, A.,* Bubble formation and its movement in Newtonian and non-Newtonian liquids, in Encyclopedia of Fluid Mechanics, (*Cheremisinoff, N. P.* (Ed.)), Vol. 3, Gulf Pub. Co., Houston, TX, 1986, pp. 58–88.
5. *Acharya, A., Mashelkar, R. A., Ulbrecht. J. J.,* Ind. Eng. Chem. Fundam. **17** (1978) 230. http://dx.doi.org/10.1021/i160067a018
6. *Acharya, A., Ulbrecht, J. J.,* AIChE J. **24** (1978) 348. http://dx.doi.org/10.1002/aic.690240227
7. *Miyahara, T., Wang, W. H., Takahashi, T.,* J. Chem. Eng. Jpn. **21** (1988) 620. http://dx.doi.org/10.1252/jcej.21.620
8. *Terasaka, K., Tsuge, H.,* Chem. Eng. Sci. **46** (1991) 85. http://dx.doi.org/10.1016/0009–2509(91)80119-J
9. *Terasaka, K., Tsuge, H.,* AIChE J. **43** (1997) 2903. http://dx.doi.org/10.1002/aic.690431103
10. *Terasaka, K., Tsuge, H.,* Chem. Eng. Sci. **56** (2001) 3237. http://dx.doi.org/10.1016/S0009–2509(01)00002–1
11. *Li, H. Z.,* Chem. Eng. Sci. **54** (1999) 2247. http://dx.doi.org/10.1016/S0009–2509(98)00294–2
12. *Li, H. Z., Mouline, Y., Midoux, N.,* Chem. Eng. Sci. **57** (2002) 339. http://dx.doi.org/10.1016/S0009–2509(01)00394–3
13. *Favelukis, M., Albalak, R. J.,* Chem. Eng. J. **63** (1996) 149.
14. *Burman, J. E., Jameson, G. J.,* Int. J. Heat Mass Transfer **21** (1978) 127. http://dx.doi.org/10.1016/0017–9310(78)90215–6
15. *Martín, M., Montes, F. J., Galán, M. A.,* Chem. Eng. Sci. **61** (2006) 363. http://dx.doi.org/10.1016/j.ces.2005.06.018
16. *Martín, M., Montes, F. J., Galán, M. A.,* Chem. Eng. Sci. **61** (2006) 5196. http://dx.doi.org/10.1016/j.ces.2006.03.027
17. *Fan, W. Y., Jiang, S. K., Zhu, C. Y., Ma, Y. G., Li, H. Z.,* Opt. Laser Technol. **40** (2008) 389. http://dx.doi.org/10.1016/j.optlastec.2007.07.002
18. *Vélez-Cordero, J. R., Zenit, R.,* J. Non-Newtonian Fluid Mech. **166** (2011) 32. http://dx.doi.org/10.1016/j.jnnfm.2010.10.003
19. *Hassagar, O.,* Nature **279** (1979) 402. http://dx.doi.org/10.1038/279402a0
20. *Bisgaard, C., Hassager, O.,* Rheol. Acta **21** (1982) 537. http://dx.doi.org/10.1007/BF01534341
21. *Arigo, M. T., McKinley, G. H.,* Rheol. Acta **37** (1998) 307. http://dx.doi.org/10.1007/s003970050118
22. *Frank, X., Li, H. Z.,* Phys. Rev. E. **71** (2005) 036309. http://dx.doi.org/10.1103/PhysRevE.71.036309
23. *Frank, X., Li, H. Z.,* Phys. Rev. E. **74** (2006) 056307. http://dx.doi.org/10.1103/PhysRevE.74.056307
24. *Kemiha, M., Frank, X., Poncin, S., Li, H. Z.,* Chem. Eng. Sci. **61** (2006) 4041. http://dx.doi.org/10.1016/j.ces.2006.01.051
25. *Pillapakkam, S. B., Singh, P., Blackmore, D., Aubry, N.,* J. Fluid Mech. **589** (2007) 215. http://dx.doi.org/10.1017/S0022112007007628
26. *Sousa, R. G., Pinto, A. M. F. R., Campos, J. B. L. M.,* Int. J. Multiphase Flow **33** (2007) 970. http://dx.doi.org/10.1016/j.ijmultiphaseflow.2007.03.009
27. *Lin, T. J., Lin, G. M.,* Chem. Eng. J. **155** (2009) 750. http://dx.doi.org/10.1016/j.cej.2009.09.019
28. *Fan, W. Y., Ma, Y. G., Li, X. L., Li, H. Z.,* Chin. J. Chem. Eng. **17** (2009) 904. http://dx.doi.org/10.1016/S1004–9541(08)60295–5
29. *Zhang, L., Yang, C., Mao, Z. S.,* J. Non-Newtonian Fluid Mech. **165** (2010) 555. http://dx.doi.org/10.1016/j.jnnfm.2010.02.012
30. *Li, S. B., Ma, Y. G., Fu, T. T., Zu, C. Y., Li, H. Z.,* Braz. J. Chem. Eng. **29** (2012) 265. http://dx.doi.org/10.1590/S0104–66322012000200007
31. *Li, S. B., Ma, Y. G., Fu, T. T., Zu, C. Y., Li, H. Z.,* Chin. J. Chem. Eng. **20** (2012) 883. http://dx.doi.org/10.1016/S1004–9541(12)60413–3
32. *Amirnia, S., de Bruyn, J. R., Bergougnou, M. A., Margaritis, A.,* Chem. Eng. Sci. **94** (2013) 60. http://dx.doi.org/10.1016/j.ces.2013.02.032
33. *Kumara, W. A. S., Elseth, G., Halvorsen, B. M., Melaaen, M. C.,* Flow Meas. Instrum. **21** (2010) 105. http://dx.doi.org/10.1016/j.flowmeasinst.2010.01.005
34. *Liu, Z. L., Zheng, Y., Jia, L. F., Zhang, Q. K.,* Chem. Eng. Sci. **60** (2005) 3537. http://dx.doi.org/10.1016/j.ces.2004.03.049